Nuclear Engineering and Design 295 (2015) 457–467

Contents lists available at ScienceDirect

Nuclear Engineering and Design

journal homepage: www.elsevier.com/locate/nucengdes

Structural integrity assessments of steam generator tubes using the FAD methodology

Marcos A. Bergant[a,*], Alejandro A. Yawny[b], Juan E. Perez Ipiña[c]

[a] Gerencia CAREM, Centro Atómico Bariloche (CNEA), Av. Bustillo 9500, San Carlos de Bariloche 8400, Argentina
[b] División Física de Metales, Centro Atómico Bariloche (CNEA)/CONICET, Av. Bustillo 9500, San Carlos de Bariloche 8400, Argentina
[c] Grupo Mecánica de Fractura, Universidad Nacional del Comahue/CONICET, Buenos Aires 1400, Neuquén 8300, Argentina

HIGHLIGHTS

- The Failure Assessment Diagram (FAD) is used to assess cracked steam generator tubes.
- Typical loading conditions and reported tensile and fracture properties are used.
- The FAD is capable to predict the failure mode for different cracks and loads.
- The FAD can be used to reduce the conservatism of the current plugging criteria.
- Appropriate tensile and fracture properties at operating conditions are required.

ARTICLE INFO

Article history:
Received 22 December 2014
Received in revised form 23 June 2015
Accepted 15 September 2015

ABSTRACT

Steam generator tubes (SGTs) represents up to 60% of the total primary pressure retaining boundary area of a nuclear power plant. They have been found susceptible to diverse degradation mechanisms during service. Due to the significance of a SGT failure on the plant safe operation, nuclear regulatory authorities have established tube plugging or repairing criteria which are based on the defect depth. The widespreadly used "40% criterion" proposed in the 70s is an example whose use is still recommended in the last editions of the ASME Boiler and Pressure Vessel Code. In the present work, an alternative, more realistic and less conservative methodology for SGT integrity evaluation is proposed. It is based on the Failure Assessment Diagram (FAD) and takes advantage of the recent developments in non-destructive techniques which allow a more comprehensive characterization of tube defects, i.e., depth, length, orientation and type. The proposed approach has been applied to: the study of the influence of primary and secondary stresses on tube integrity; the prediction of failure mode (i.e., ductile fracture or plastic collapse) of defective SGTs for varied crack geometries and loading conditions; the analysis of the sensibility of tensile and fracture properties with temperature. The potentiality of the FAD as a comprehensive methodology for predicting the failure loads and failure modes of flawed SGTs is highlighted.

1. Introduction

Steam generators (SGs) are shell and tube heat exchangers that use the heat produced in a nuclear reactor core to convert liquid water into steam. The SGs are basically tube bundles arranged inside a pressure vessel, where the thin-walled tubes act as the physical barrier between the primary and secondary coolant circuits. Although the number of SG tubes (SGTs) may vary significantly depending the SG design (the number of tubes can reach several thousand per SG) the tubing walls can comprise up to 60% of the total primary pressure retaining boundary area. If a rupture of the tube walls occurs, the primary water at higher pressure will leak to the secondary circuit with a potential release of radioactivity.

As the principal function of the SGs is the heat removal from the reactor core, the assurance of their continuous operation is a relevant issue concerning the plant safety during certain events or accident conditions.

During long-term operation varied degradation mechanisms (i.e., stress corrosion cracking or other corrosion mechanisms, fretting fatigue and fretting wear) may introduce structural defects affecting the integrity of the SGTs. These defects can promote

* Corresponding author. Tel.: +54 294 444 3846.
E-mail addresses: marcos.bergant@cab.cnea.gov.ar (M.A. Bergant), yawny@cab.cnea.gov.ar (A.A. Yawny), juan.perezipina@fain.uncoma.edu.ar (J.E. Perez Ipiña).

http://dx.doi.org/10.1016/j.nucengdes.2015.09.022
0029-5493/

Nomenclature

a	depth of surface crack-like flaw
c	half length of through-wall crack-like flaw
EPFM	elastic plastic fracture mechanics
F	force
FAD	failure assessment diagram
J	J-integral
J_q	J-integral at stable crack growth initiation
K	stress intensity factor
K_I^P	mode I stress intensity factor based on primary stresses
K_I^S	mode I stress intensity factor based on secondary stresses
K_{mat}	fracture toughness of material
K_r	toughness ratio
LEFM	linear elastic fracture mechanics
L_r	load ratio
$L_{r\,max}$	cut-off value of the load ratio
P	pressure
P_b	primary bending stress
P_m	primary membrane stress
PTWC	part-through-wall crack
R_0	outside tube radius
R_i	inside tube radius
RT	room temperature
SG	steam generator
SGT	steam generator tube
σ_C^S	circumferential primary stress
σ_C^S	circumferential secondary stress
σ_f	flow stress
σ_L^P	longitudinal primary stress
σ_L^S	longitudinal secondary stress
σ_{ref}	reference stress
σ_u	ultimate tensile strength
σ_{ys}	yield strength
ϕ	plasticity interaction factor
T	temperature
t	tube thickness
TWC	through-wall crack

failures such as tube burst and crack opening, leading to unacceptable leak rates. Remediation is usually performed by plugging the failed tube with a consequent reduction of the thermal efficiency of the plant. If the number of plugged tubes increases sufficiently, the replacement of the whole SG unit is required, involving costs of hundreds of million dollars (Abou-Hanna et al., 2004). Hence, the structural integrity assessment of defective SGTs has an essential importance from the safety and economic perspectives.

Consequently, a significant research effort has been made in the last decades resulting in considerable improvements in the resistance to cracking problems due to corrosion or fretting phenomena. The aim of these researches was the prevention of cracking. However, once the cracks are present, the assessment of their significance is still an open issue, mainly due to the lack of representative fracture toughness data of SGTs in operating conditions.

The nuclear industry has developed regulatory requirements in order to ensure a low probability of spontaneous SGTs failures under both normal and accident conditions. Nevertheless, the experience has shown that these former criteria can be excessively conservative, i.e., its application resulting in a high number of tubes unnecessarily plugged.

In the present work, the use of the Failure Assessment Diagram (FAD) for the assessment of the structural integrity of cracked SGTs is proposed. Typical loading conditions, crack types and tensile and fracture properties of actual SGTs reported in literature are analyzed. It is shown how the proposed methodology may result in an improved repair and plugging criteria formulation.

2. Structural integrity assessment approaches for flawed SGTs

One of the most widely implemented repair or plugging criteria in use is the one published in the US Code of Federal Regulations and in the ASME Pressure Vessel and Boiler Code, i.e., the so-called "40% criterion". It establishes that the allowable depth of a defect should be less than 40% of the tube wall thickness. As the non-destructive technique (NDT) used for in service inspection, i.e., the eddy current method, gives the depth of the degradation as the main result of the examination, the traditional tube repair or plugging criteria is based on a minimum wall thickness requirement.

The minimum wall thickness is determined from integrity assessments based on plastic limit loads analyses performed with safety margins against tube pressure bursting for postulated loads under normal and accident conditions (IAEA, 2007). Only the pressure difference across the tube wall is considered as the postulated load. Inconel 600 SGTs 3/4″ and 7/8″ in diameter were analyzed in this way (IAEA, 2007).

Although the "40% criterion" is still widely used in the nuclear industry, it is often applied without a clear understanding of the limitations related with the assumptions made for its formulation. This results in excessive conservatism and to overcome these drawbacks, the ASME code permits the use of alternative criteria subjected to previous acceptance by the regulatory authorities.

Therefore, with the purpose of reducing the number of tubes that were unnecessarily removed from service, new revised fitness for service criteria was recently proposed in the open literature. They include both generic type (e.g., less conservative minimum thickness approaches) and defect type or location specific criteria (i.e., those used for volumetric or planar crack-like defects, located in particular areas of the SGT bundle) (IAEA, 2011).

Most of the proposed criteria are based on limit load analysis where plastic collapse is the prevailing mode of failure (Flesch and Cochet, 1990; Lee et al., 2001; Majumdar, 1999b; Tonkovic et al., 2008). This is a reasonably assumption considering the significant ductility of the typical SGT materials. Although these methods are easy to implement because of the availability of limit load expressions for different cracked geometries and loading conditions, the choice of a particular flow stress for the material considered was shown to affect the estimated values (Tonkovic et al., 2008). Therefore, limit load analyses seem to be simple to apply in practice, but need extensive supporting experimental data and still further research in order to validate their applicability.

On the other hand, methodologies based on fracture mechanics have been proposed for assessing the structural integrity of cracked SGTs. Both linear elastic fracture mechanics (LEFM) and elastic plastic fracture mechanics (EPFM) were considered (Chang et al., 2006; Cizelj et al., 1995; Huh et al., 2006; Majumdar, 1999a; Park et al., 2002; Tonkovic et al., 2005; Wang and Reinhardt, 2003). These analyses can be easily generalized to different loading conditions without the need of additional experimental validation, but have a common disadvantage, i.e., the difficulties associated with the appropriate experimental evaluation of the fracture toughness of SGTs (Bergant et al., 2012).

Other authors (Bergant et al., 2015; Chang et al., 2006; Lee et al., 2001; Tonkovic et al., 2008; Wang and Reinhardt, 2003) have proposed the FAD method as a more comprehensive alternative capable of encompassing both limit load and fracture mechanics assessments in a single analysis. In support of this, it is worth

Table 1
Tensile and fracture toughness properties of SGTs at RT reported in literature.

Reference	SGT alloy	σ_{ys} (MPa)	σ_u (MPa)	Crack orientation	J_q (kJ/m^2) (lower bound)	K_{mat} (MPa m$^{1/2}$)
Huh et al. (2006)	Inconel 600 (9Fe–74Ni–16Cr)	259	668	Circumferential	471	317
Bergant et al. (2012)	Incoloy 800 (42Fe–33Ni–22Cr)	260	610	Circumferential	717	375
Sanyal and Samal (2013)	Incoloy 800 (46Fe–32Ni–20Cr)	210	500	Longitudinal	250	222

mentioning here that Section XI of the ASME code permits the use of the FAD methodology for the structural assessment of cracked tubing made of austenitic materials. Besides that, the FAD approach has been included in many structural integrity assessment procedures of the most important codes and guides (e.g., ASME Section XI, API 579-1/ASME FFS-1, SINTAP and BS 7910). Thus, it is expected that FAD will become more familiar for most structural engineers in the short term.

In a previous work (Bergant et al., 2015), some preliminary conclusions were obtained from integrity assessments of flawed SGTs using the FAD approach. The present work is a continuation and completion of that, where new analyses are presented. Secondary stresses due to differential thermal expansion are estimated and incorporated in the FAD assessment, in order to appraise their effect on the stability of crack-like defects. Also, the impact of the typical reduction of tensile properties from room temperature (RT) to operating conditions is analyzed numerically for different SGT materials. Finally, numerical results of the FAD application to flawed SGTs are presented.

3. Experimental data of fracture toughness properties of SGTs

The application of the FAD analysis for SGT structural integrity evaluation requires the previous characterization of the tensile and fracture toughness properties of the tube material in its final microstructural condition. The restrictive geometry of SGTs prevents using standardized fracture specimens in order to assure plane strain conditions considering the inherent high toughness of the austenitic alloys used in SGTs. Therefore, alternative non-standardized test techniques based on EPFM are required.

A summary of three researches available in the open literature dealing with the experimental determination of fracture toughness of SGTs was presented in a previous work (Bergant et al., 2015). Readers interested in more details are requested to consult the original works of Bergant et al. (2012), Huh et al. (2006) and Sanyal and Samal (2013). Here, only the main results extracted from the mentioned works, including the yield strength σ_{ys} and the ultimate tensile strength σ_u are presented in Table 1. The fracture toughness of Incoloy 800 annealed and Inconel 600 were evaluated at RT. Though toughness were evaluated in terms of J-resistance tests, only values corresponding to stable crack growth initiation J_q are included. Longitudinal and circumferential through-wall cracks were used in the tests. The equivalent linear elastic parameter K_{mat} calculated from the J_q value through the correspondence between K and J will be used for integrity assessments in the present work (Anderson, 2005). It should be noted the marked difference between the fracture toughness values reported in Bergant et al. (2012) and Sanyal and Samal (2013) using similar SGT material. This result can be attributed to an anisotropy effect on the fracture properties of Incoloy 800 annealed tubes and the different crack orientation considered, i.e., circumferential and longitudinal, respectively. Although anisotropy in tensile properties is also expected, Table 1 presents only the typical longitudinal tensile data reported in the original works.

Although others authors performing SGTs structural integrity assessment (Chang et al., 2006; Hu et al., 2011; Tonkovic et al., 2005, 2008; Wang and Reinhardt, 2003; Wilam and Cermakova, 1995) have reported fracture toughness values for similar materials, the specific details of their experimental determination were not provided. As this cast some doubts about their strict validity, these values were not considered in the present work.

More accurate structural integrity assessments would therefore require additional experimental effort in assessing the fracture properties of SGTs. A comprehensive testing program should include investigation of the effects of the specific alloy (e.g., Incoloy 800 or Inconel 600 and 690), crack orientation (e.g., circumferential or longitudinal) and typical operating temperatures.

4. Structural integrity assessments based in the FAD approach

4.1. The FAD methodology

The high fracture toughness values characteristics of austenitic materials indicated in Table 1 suggest that the failure mechanism of SGTs may lie between ductile fracture and plastic collapse of the remaining ligament. In this context, the FAD approach arises as the appropriate assessment technique due to its versatility, being applicable to a wide range of material behaviors ranging from brittle fracture under linear elastic conditions to ductile overload in the fully plastic regime. Furthermore, the FAD methodology is easy to implement, requiring the use of only two parameters that vary linearly with the applied load. As an additional advantage, FAD can easily deal with cracked components when primary, secondary or residual stresses are present (Anderson, 2005). Secondary stresses usually include displacement-controlled loads, such as differential thermal expansion. The basic characteristic of secondary stresses is that they are self-equilibrating over the entire structure. Whereas their contribution to plastic collapse of a component is normally not considered, secondary stresses affect the fracture driving force; therefore, they must be included in an integrity assessment.

As mentioned before, the FAD methodology requires the evaluation of two parameters. They are the toughness ratio K_r and the load ratio L_r that define the coordinates of an assessment point in the FAD diagram whose position relative to a failure line determines the safety margin of the component. This line represents the failure locus and all points at the left down side of the line are considered safe (Anderson, 2005). The evaluation of these two parameters and the construction of the failure line are explained in more detail in what follows.

The toughness ratio K_r is based on LEFM parameters and is computed as:

$$K_r = \frac{K_I^P + \phi K_I^S}{K_{mat}} \quad (1)$$

where, K_I^P and K_I^S are the Mode I stress-intensity factors due to primary and secondary stresses, respectively, and K_{mat} is the material fracture toughness. ϕ is the plasticity interaction factor that can be interpreted as an adjustable parameter to take into account crack tip plasticity effects (Anderson, 2005). When linear elastic conditions prevail, secondary and primary stresses are treated in the same fashion and $\phi = 1$. At intermediate applied stresses, the plastic interaction between primary and secondary stresses increases the total fracture driving force and $\phi > 1$, reaching a maximum value. If higher stresses are applied, the plasticity developed at the crack tip

due to the combination of primary and secondary stresses lead to the redistribution and relaxation of secondary stresses. This gives rise to a mechanical stress relief effect and, accordingly, ϕ tends to decrease even reaching values $\phi < 1$. In the fully plastic regime, the relaxation of secondary stresses becomes complete and the fracture driving force tends to depend only on primary stresses.

The load ratio L_r is based on the parameters determining plastic collapse and is calculated as:

$$L_r = \frac{\sigma_{ref}}{\sigma_{ys}} \tag{2}$$

where, σ_{ref} is a reference stress and σ_{ys} is the yield strength. The stress σ_{ref} can be thought as the effective primary stress acting in the net area, and is based on limit load solutions for the configuration of interest. The maximum load ratio $L_{r\,max}$ is a cut-off value representing a limit load criterion (Anderson, 2005).

Three options of FAD diagrams with respective definitions of failure lines were developed (Anderson, 2005). The first option is a lower bound FAD of generic shape, independent of the material and component geometry under assessment. The second option is a material specific FAD diagram, which can be constructed if stress–strain curves are available. Finally, the third option is a *J*-based FAD that incorporates both the component geometry and material effects. From the first to the third option, the FAD curve definition becomes more detailed and complex, while the accuracy of the assessments improves and the degree of conservatism decreases. As this work is an initial attempt to apply the FAD approach to the evaluation of the structural integrity of SGTs and given that fracture properties at RT are used, the first option, i.e., the generic shape FAD is considered for further analysis:

$$K_r(L_r) = \left(1 - 0.14L_r^2\right)\left(0.3 + 0.7e^{-0.65L_r^6}\right). \tag{3}$$

Eq. (3) corresponds to the first option for K_r vs. L_r estimation proposed in API 579-1/ASME FFS-1 and R6-Revision 3 guides.

4.2. Structural integrity assessment of SGTs using the FAD: basic hypothesis

In the following sections, examples of structural integrity assessments of flawed SGTs based on the FAD approach are presented. In order to perform comparisons with experimental data using the fracture properties of Table 1, two typical SGT geometries were adopted. Thereby, tubes of Incoloy 800 annealed (with 15.88 mm and 1.13 mm for outside diameter and wall thickness, respectively) and tubes of Inconel 600 (with 19.05 mm and 1.09 mm for outside diameter and wall thickness, respectively) were considered.

The crack driving forces were calculated using the API 579-1/ASME FFS-1 (2007) procedure. Appendices A and B summarize the equations used for calculating the parameters K_I, ϕ and σ_{ref} of Eqs. (1) and (2). A generic shape FAD option was used, while the stable crack growth initiation was adopted as the failure condition for fracture. Therefore, fracture toughness values for crack growth initiation K_{mat} were used in Eq. (1). It should be noted that the crack growth initiation criterion can be adequate to prevent part through-wall cracks (PTWCs) resulting in leaks, i.e., to become through-wall cracks (TWCs) taking into account the typical thin walls of SGTs. However, this failure criterion can be conservative for predicting unstable crack growth that leads to the tube burst. The flow stress σ_f was estimated as $1.15(\sigma_{ys} + \sigma_u)/2$, which is the value recommended for austenitic materials (API 579-1/ASME FFS-1, 2007). Then, the cut-off value $L_{r\,max}$ was calculated as σ_f/σ_{ys}, giving approximately 2.

Both PTWCs and TWCs were included in the present study. Although under normal operation conditions TWCs are assumed to be unacceptable due to their tendency to produce leakage from the primary to the secondary circuits, there are some reasons that justify their consideration. TWCs can be present during normal operation as long as they result either in a very tight leakage which is inferior to the detection threshold of the on-line leak rate monitoring systems or in a leak rate below the typical operational limit per SG (technical specifications). Additionally, some European countries are implementing specific repairing criteria based only on crack lengths, accepting even TWCs for continued service (IAEA, 2011).

Also, it is well known that the depths of PTWCs can be significantly more difficult to estimate than their respective lengths. In such cases, their consideration as TWCs is a convenient conservative assumption. On the other hand, flaw indications obtained through NDT have usually an irregular shape and environmental cracks (i.e., those due to SCC mechanisms) are typically multiple and branched. Therefore, assessment procedures can be applied to such cracks provided a predominant crack whose behavior largely controls the structural response of the component can be identified. Thus, different characterization rules were developed leading to idealized crack geometries more amenable to fracture mechanics analyses. They account for flaw shape, orientation and interaction. Even when actual cracks are not TWCs, the application of the characterization rules often result in TWCs or deep predominant cracks. As an example, API 579-1/ASME FFS-1 recommends to reclassify flaws with $a/t > 0.8$ as TWCs. This is because for deep surface flaws where the remaining ligament is small, the high strain levels and plasticity effects produce inaccurate results for both stress intensity factor and reference stress solutions. In fact, it is noticed in API 579-1/ASME FFS-1 that the reference stresses in the remaining ligament may be overestimated in the case of deep flaws, resulting in the assessment point falling in the failure region of the FAD. Recategorization of a surface flaw to a TWC may result in the associated assessment point being inside of the failure assessment line.

Therefore, given that the SGTs materials have considerably high fracture toughness and work hardening rate, it is likely that the expected limiting flaws are large enough, allowing them to be modeled as TWCs. Also the assessments of TWCs in SGTs are of interest for leak-before-break (Flesch and Cochet, 1990) and leak rate analyses (Erhard et al., 2012).

4.3. FAD assessments for SGTs with primary and secondary stresses

As the aim of the present work was to assess on the significance of crack-like defects in SGTs under typical loading conditions, two loading sources that are always present in SGTs are considered. They are the pressure difference across the tube wall, which promotes primary stresses, and the differential thermal expansion through the tube wall, leading to secondary stresses.

Several elastic solutions for both problems are available in technical literature (Timoshenko and Goodier, 1970), concluding that only the circumferential and longitudinal components of the stress tensors are relevant given that the radial component is much lower. For assessment of primary stresses, a thick wall cylindrical shell capped with free ends was assumed. Pressure differences, $\Delta P = P_{int} - P_{ext}$, of 9 and 27 MPa were considered. These are the typical values adopted for normal and accident conditions in SGTs, as will be seen later (Majumdar, 1999b). In the case of thermal stresses, a steady state condition is assumed that defines a radial temperature gradient. This gradient depends only on the tube geometry and on the temperature difference across the tube wall, $\Delta T = T_{int} - T_{ext}$. Typically, ΔT varies with the location inside the SG. For that reason, three ΔT values were considered, i.e., 0, 50 and 100 °C, in order to cover the range of typical values for PWR SGs (Green and Hetsroni, 1995). Fig. 1(a) and (b) shows the variation

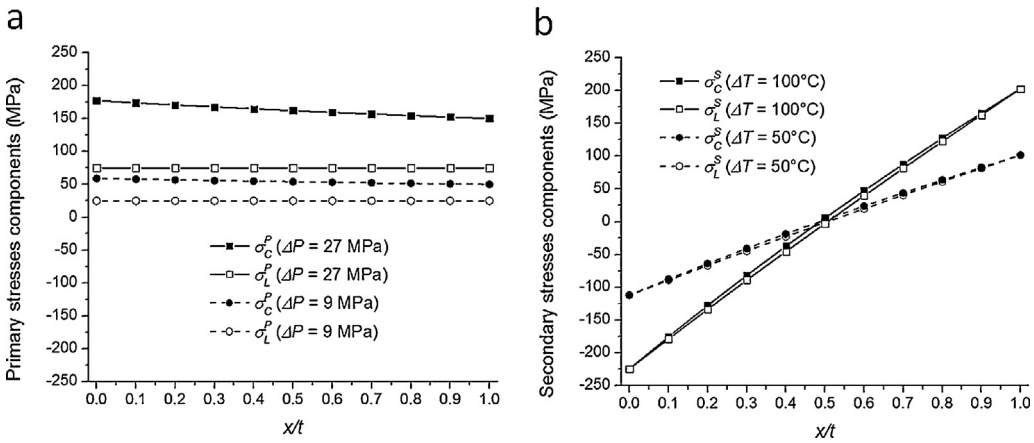

Fig. 1. Typical primary and secondary stresses in SGTs due to (a) pressure difference and (b) thermal stresses.

of the primary and secondary stresses components for $\Delta P = 9$ and 27 MPa (with $\Delta T = 0\,^{\circ}C$), and $\Delta T = 50$ and $100\,^{\circ}C$ (with $\Delta P = 0$ MPa), respectively, in terms of the radial coordinate along the tube wall x/t (Timoshenko and Goodier, 1970). The primary circuit was supposed in the inner side of the tube ($x/t = 0$). The circumferential and longitudinal stresses components were denoted as σ_C and σ_L, respectively. An Incoloy 800 tube with 15.88 mm outside diameter and 1.13 mm wall thickness was considered. Equations in Appendices A.1, A.2, B, B.1 and B.2 were used to evaluate the (L_r, K_r) points in the FAD. Analysis of Fig. 1(b) indicates that thermal stresses reach maximum values as high as the yield stress. Their self-equilibrating character can also be appreciated. Little difference exists between the components σ_C^S and σ_L^S for a given ΔT.

It is worth mentioning that the thermal stresses considered here are compressive in the inner part of the tube wall. Therefore, if a crack tip is located in this side, the fracture driving force due to secondary stresses is negative thus reducing the total driving force. However, the API 579-1/ASME FFS-1 guide suggests in this case setting $K_I^S = 0$ in order to perform a conservative assessment.

With the aim of comparing the effect of both stresses, tubes with semi-elliptical PTWCs and TWCs in a longitudinal plane subjected to internal pressure and thermal stresses were investigated. The PTWC was located in the outer side of the tube, so tensile thermal stresses were analyzed. For the TWC, the stress intensity factors K_I^P and K_I^S were calculated in the outer point (Fig. 2).

For a given crack geometry, when the primary load or pressure is increased, the assessment points in the FAD move following a line, called the loading line. The intersection of the loading line and the FAD failure curve determines the condition (i.e., the load level) for the component failure. In the absence of secondary stresses, the loading path is a straight line with a slope defined by the cracked component geometry and the type of loading (i.e., internal pressure, tensile or bending loads, etc.). When secondary stresses are added (presence of ΔT values), the fracture driving force K_r is incremented resulting in a higher loading line as it is shown in Fig. 2 for increasing values of ΔT.

Three levels of thermal stresses corresponding to $\Delta T = 0\,^{\circ}C$, $50\,^{\circ}C$ and $100\,^{\circ}C$ have been considered. When their respective secondary stresses are added, the fracture driving force K_r is incremented resulting in a higher loading lines as it can be appreciated by the dashed ($\Delta T = 50\,^{\circ}C$) and dotted ($\Delta T = 100\,^{\circ}C$) lines included in Fig. 2 for both TWC (upper set of loading paths) and PTWC (lower set of loading paths).

The case $\Delta T = 0\,^{\circ}C$ corresponds to null secondary stresses or, in other words, to the assessment with only primary stresses due to internal pressure. It can be seen that the relative importance of secondary stresses diminishes as the primary load applied increases, i.e., at higher L_r ratios. This is due to the mechanical stress relief mentioned previously (decreasing ϕ factor). Since the failure condition given by the L_r coordinate of the intersection between the loading paths and the failure line is only weakly affected by the presence of secondary stresses, it can be concluded that typical thermal stresses developed in PWR SGTs are second order in the structural integrity assessment of crack-like flaws. Equivalent

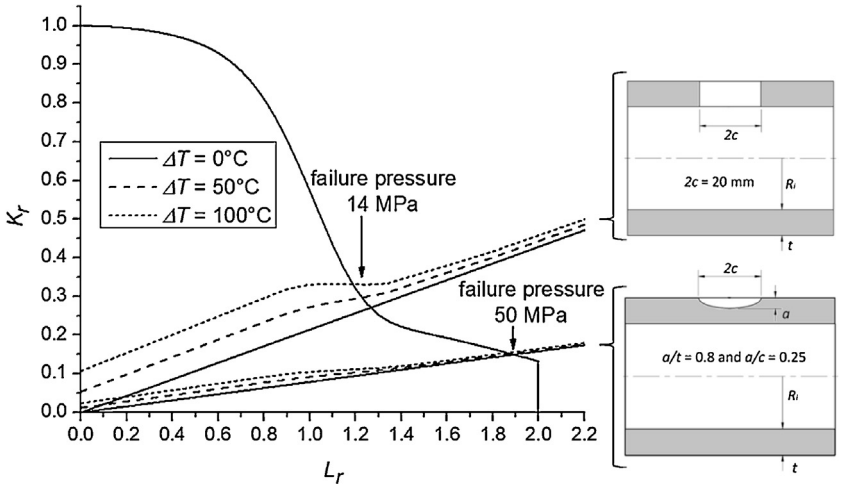

Fig. 2. FAD assessments for TWC and PTWC including primary and secondary stresses induced by different temperature differences ΔT along the tube wall.

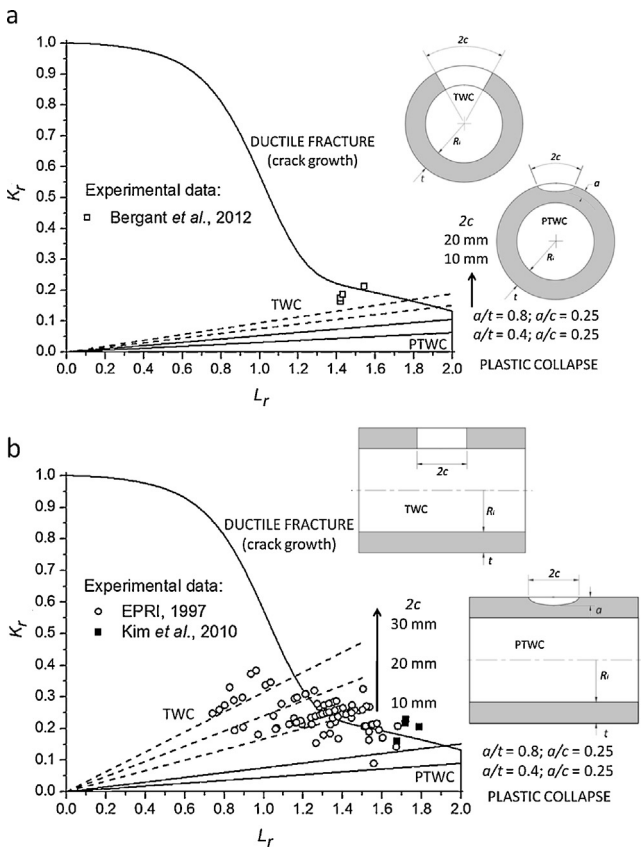

Fig. 3. FAD assessments in SGTs. (a) Circumferential cracks, tube loaded in tension (normal to the paper) with K_{mat} = 375 MPa m$^{1/2}$. (b) Longitudinal cracks in a tube under internal pressure with K_{mat} = 222 MPa m$^{1/2}$.

results can be obtained for different crack geometries. Therefore, an important conclusion can be drawn from the previous analysis, i.e., primary stress components are the controlling driving forces for SGTs cracked related failures. The same conclusion was found experimentally (Flesch and Cochet, 1990).

4.4. Failure mode prediction using the FAD

Fig. 3(a) shows the FAD for circumferential cracks in a SGT under tensile load assuming K_{mat} = 375 MPa m$^{1/2}$ while Fig. 3(b) refers to longitudinal cracks in a tube under internal pressure where K_{mat} = 222 MPa m$^{1/2}$. Mechanical properties of Incoloy 800 tubes in Table 1 were used, with 15.88 mm and 1.13 mm for outside diameter and wall thickness, respectively. Both semi-elliptical PTWCs and TWCs were considered and for the sake of clarity, thermal stresses were not included in the analysis. Appendices A.1, A.2, A.3 and A.4 present the expressions used to estimate the assessment points.

Fig. 3(a) also presents experimental data from tensile fracture tests performed in Incoloy 800 tubes with circumferential TWCs at RT (Bergant et al., 2012). The points (L_r, K_r) represent the onset of stable crack growth obtained using fracture and mechanical properties for Incoloy 800 and considering circumferential cracks in Table 1. On the other hand, Fig. 3(b) shows experimental data from burst tests of Inconel 600 tubes with longitudinal TWCs at RT (EPRI, 1997; Kim et al., 2010). The points (L_r, K_r) were calculated using the mechanical properties and tube geometries reported in the references, while a K_{mat} = 317 MPa m$^{1/2}$ from Table 1 for Inconel 600 was adopted. It is believed that the dispersion in (L_r, K_r) points from data of EPRI (1997) comes from the diversity of mechanical properties and tube geometries tested. Although σ_f is provided for all the tested tubes, only a mean value for σ_{ys} is reported. Therefore, the L_r coordinates (Eq. (2)) are not well defined, contributing to the spread of experimental data points. Despite this, a general good agreement is observed between experiments and the predictions derived from the FAD approach.

From the analytical results, it can be seen that for circumferential cracks and material with the highest fracture toughness, the failure mode predicted by the FAD is close to plastic collapse. This is particularly evident in the case of the semi-elliptical PTWC short cracks. On the other hand, for relative large longitudinal cracks and material with the lowest fracture toughness, the failure mechanism falls in the region dominated by interacting fracture and plastic collapse. It is worthwhile noting here that in the last case, a solely plastic collapse analysis will give a non-conservative prediction of the failure condition.

4.5. Conservatism of traditional plugging/repairing criteria

As was already mentioned, the traditional minimum wall plugging criterion in the ASME code, the "40% criterion", has been demonstrated to be excessively conservative (IAEA, 2011). This high degree of conservatism can be better appreciated by applying both the here proposed FAD approach and the "40% criterion" to a representative case. A cracked tube with differential pressure ΔP as the primary loading condition is considered. Under normal operating conditions, the pressure across a typical PWR SGT wall ΔP_{NO} is about 9 MPa. Under accident conditions (e.g., steamline break in which the secondary side has dropped to atmospheric pressure), the differential pressure can increase from the normal operation value to ΔP_{ACC} = 18 MPa. According to the ASME code, defective tubes must actually be capable of withstanding 3 × ΔP_{NO} (27 MPa) or 1.43 × ΔP_{ACC} (26 MPa), whichever is higher, for continued safe operation (Majumdar, 1999b).

Flesch and Cochet (1990) presented experimental data of burst tests of Inconel 600 tubes with longitudinal PTWCs. In order to use these data, the geometry and mechanical properties of reported tests were adopted in the present analysis (i.e., 19.05 mm and 1.09 mm for outside diameter and wall thickness, respectively, and σ_{ys} = 331 MPa and σ_u = 717 MPa). The fracture toughness K_{mat} = 317 MPa m$^{1/2}$ for Inconel 600 in Table 1 was used. A conservative assessment is performed by assuming an internal infinite longitudinal PTWC (40% of tube wall depth) in a tube subjected to an internal pressure of 27 MPa. Appendix A.5 presents the expressions used to calculate the (L_r, K_r) coordinates. The FAD for the above conditions is constructed in Fig. 4. It can be seen that the assessment point corresponding to a relative crack depth a/t = 0.4 falls behind the failure line, thus representing a safe condition. The FAD methodology predicts the failure would occur by plastic collapse when the crack depth reaches 62% of the tube wall thickness. Fig. 4 presents also experimental data for long cracks and different crack depths a/t (Flesch and Cochet, 1990), showing that the FAD properly predicts the results. This example shows the conservatism of the "40% criterion", even in limiting cases as the one just analyzed. The same analysis applied to a circumferential crack (i.e., with half membrane stress due to the differential pressure and higher toughness) or to a longitudinal crack with non-infinite length would give even higher tolerable depths.

4.6. Assessment of cracked SGTs at operating temperatures: Effect of material properties

In the previous analyses, material properties determined at RT were used. However, SGTs typically operate in a range of temperatures close to 300 °C, depending on the SG design. In this section, an analysis of the effect of the material properties differences between RT and operating temperature is performed.

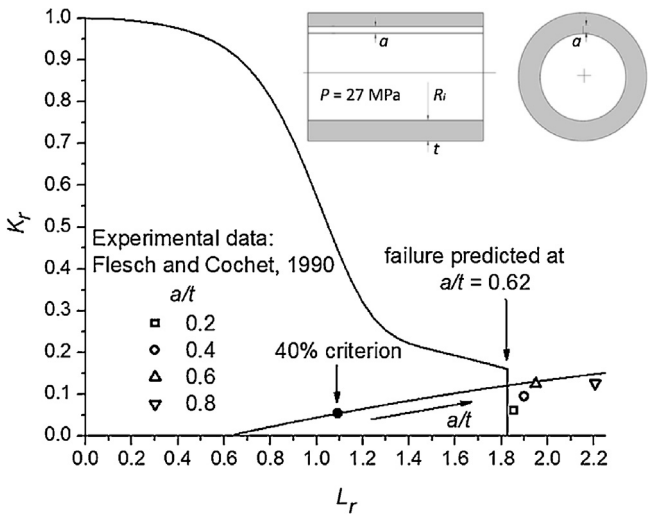

Fig. 4. Comparison between the "40% criterion" and the here proposed FAD methodology illustrating the degree of conservatism associated with the traditional approach.

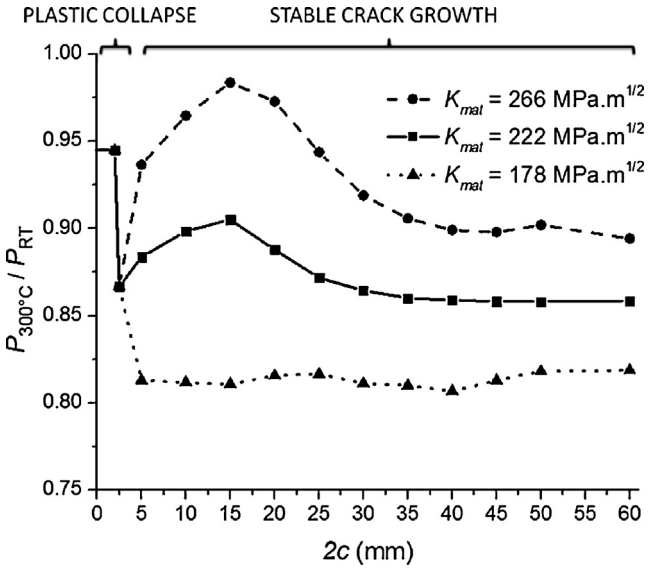

Fig. 5. Failure pressure ratios $P_{300\,^\circ C}/P_{RT}$ for longitudinal TWCs of different lengths $2c$ and different fracture toughness K_{mat} assumed for Incoloy 800 in annealed condition.

It is well known that tensile properties drop at increasing temperatures. On the other hand, the fracture toughness dependence with the temperature exhibits a less clear behavior. For instance, many austenitic stainless steels and even some ferritic steels, show a decrease in fracture toughness between 300 °C and 500 °C (ASM Handbook Vol. 19, 1997). Using standardized techniques and specimens obtained from thick plates, Mills (1987) and other researchers characterized the high temperature fracture toughness of structural nickel alloys. Mills (1987) reported an increase in resistance curves for Inconel 600 at 400 °C relative to RT, while for Incoloy 800 results indicated a decrease. These results however are not of general validity because the fracture toughness properties are strongly dependent on the thermo-mechanical condition of the material. Furthermore, in the specific case of thin walled SGTs, low constraint conditions prevail. Thus, the assumption of fracture properties obtained from thick specimens with higher degrees of constraint may result in overly conservative assessments.

Therefore, due to the lack of precise fracture toughness data for SGTs materials at operating temperatures, in the analysis that follows both possibilities have been considered, i.e., an increase and a decrease in fracture toughness with temperature. In order to obtain comparable results, the same percentage variation on tensile properties was assumed.

An Incoloy 800 tube in annealed condition (K_{mat} = 222 MPa m$^{1/2}$ at RT, Table 1) with a longitudinal TWC of length $2c$ subjected to internal pressure was considered. The outside diameter and wall thickness used were 15.88 mm and 1.13 mm, respectively. In order to simplify the analysis, thermal stresses were neglected. The Appendix A.1 presents the equations for calculating the assessment points. To account for the drop of tensile properties with temperature, the values tabulated in ASME Code Section II were used as a reference. These are minimum properties and are specific for SGTs according to the specification SB-163. For annealed Incoloy 800 SGTs, the RT and 300 °C yield strength σ_{ys} were taken as 207 and 170 MPa, respectively, representing almost a 20% reduction. For the same temperatures, the ultimate tensile strength σ_u ranges between 517 and 514 MPa. Regarding fracture toughness, a variation of ±20% in terms of K_{mat} was assumed, i.e., K_{mat} = 178, 222 and 266 MPa m$^{1/2}$.

The internal pressure leading to failure was obtained for different crack lengths $2c$. The crack lengths were varied in order to give failure modes ranging from plastic collapse for short cracks around 2 mm in length, to the beginning of stable growth in the case of longer cracks, Fig. 3(b). The estimated failure pressures at RT and 300 °C were denoted as P_{RT} and $P_{300\,^\circ C}$, respectively. Fig. 5 shows the variation of the ratio $P_{300\,^\circ C}/P_{RT}$ for different crack lengths. The three curves presented correspond each to one of the three levels of K_{mat} considered. It can be seen that for short cracks where the failure mode is plastic collapse, the pressure ratio takes a constant value around 0.94. For longer cracks, the predicted failure mode is the beginning of stable crack growth. In this case, the pressure ratio shows some dependence with the crack length. The lowest values of $P_{300\,^\circ C}/P_{RT}$ for the three curves are reached for large cracks of around 50 mm. Cracks longer than that were not analyzed because the failure pressure falls well below the typical values of operating differential pressure of SGs (i.e., ΔP_{NO} = 9 MPa), thus representing cracks not acceptable for normal operation.

The previous analysis can be easily extended to other typical SGTs alloys used in Western Power Plants. Table 2 shows the minimum yield strength σ_{ys} reported in ASME II for SGTs made of Inconel 600, Inconel 690 and Incoloy 800 alloys, with different thermo-mechanical conditions. Although SGTs of Inconel 600 are not used in new SGs due to its susceptibility to stress corrosion cracking, they have been widely used in former SGs and many tubes are still in service. Table 2 also summarizes the pressure ratios $P_{300\,^\circ C}/P_{RT}$ for plastic collapse and for the beginning of stable growth. In the later case, the pressure ratio reported corresponds to the minimum value generally obtained for long cracks, as it was shown in Fig. 5.

It can be observed that the impact of the tensile properties variation is reduced when the failure mode is plastic collapse. In this case, it is clear that the pressure ratio defined depends only on the variation of tensile properties and not on the value of K_{mat}. Given that the reference stress σ_{ref} or L_r coordinate is proportional to the applied load, this result can be extended to any crack geometry and loading condition provided the failure mode is plastic collapse. This is a relevant conclusion taking into account that many practical assessments of flawed SGTs using a FAD methodology will fall in the plastic collapse regime. This is particularly true for PTWCs, short cracks and circumferential cracks, as can be appreciated in Fig. 3(a) and (b).

When the failure mode is the beginning of stable crack growth, the pressure ratio depends both on the variation of σ_{ys} and to a minor extent on K_{mat}. The last one defines the point where the loading line and the FAD curve intersect. Fig. 6 presents the results

Table 2
Tensile properties of SGTs according to ASME II and pressure ratios for plastic collapse and stable crack growth failure modes.

SGT alloy	σ_{ys} (MPa)		$P_{300\,°C}/P_{RT}$ (plastic collapse)	Minimum $P_{300\,°C}/P_{RT}$ (stable crack growth)		
	RT	300 °C		K_{mat} = 178 MPa m$^{1/2}$	K_{mat} = 222 MPa m$^{1/2}$	K_{mat} = 266 MPa m$^{1/2}$
Inconel 600 annealed	241	207	0.957	0.84	0.89	0.92
Inconel 600 annealed HY[a]	276	237	0.953	0.85	0.89	0.93
Inconel 690 annealed	241	191	0.901	0.79	0.83	0.87
Inconel 690 annealed HY[a]	276	218	0.896	0.79	0.83	0.87
Incoloy 800 annealed	207	170	0.945	0.81	0.86	0.89
Incoloy 800 annealed HY[a]	276	226	0.933	0.81	0.86	0.89
Incoloy 800 cold-worked	324	268	0.934	0.82	0.86	0.90

[a] HY refers to high yield strength, usually obtained through grain refinement.

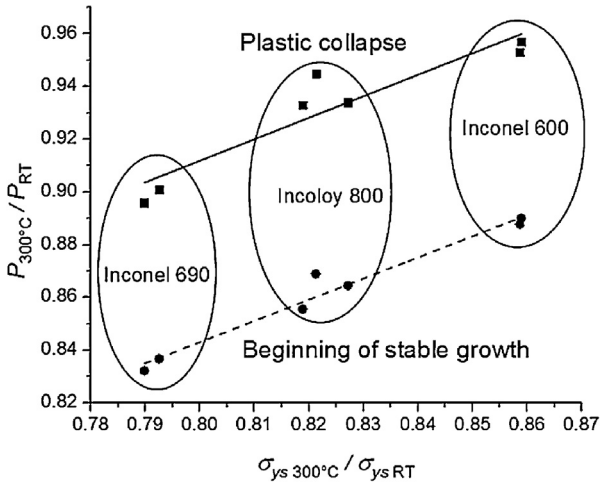

Fig. 6. Failure pressure ratios $P_{300\,°C}/P_{RT}$ for plastic collapse and beginning of stable growth. SGTs materials from Table 2 were considered.

of Table 2, showing that a linear trend exists between the pressure ratio $P_{300\,°C}/P_{RT}$ and the yield strength ratio $\sigma_{ys\ 300\,°C}/\sigma_{ys\ RT}$, defined as the quotient of the σ_{ys} at 300 °C and RT, for both plastic collapse and beginning of stable growth failure modes. This means that the limiting pressure for the failure conditions is mainly related with the yield strength variation.

If terms of percentage variations, from Table 2 it can be observed that the effect of the σ_{ys} variation on the pressure ratios is approximately 3 times higher than the variation of K_{mat} when stable crack growth initiation determines the failure condition. This result can be understood taking into account that the failure condition is closer to the plastic collapse and therefore the change in σ_{ys} has a higher relative effect than the variation of K_{mat}.

A similar analysis can be conducted in order to assess on the effect on the integrity evaluations of using tabulated minimum values in construction codes (i.e., the reported in ASME II) or actual tensile properties obtained at a given temperature. For instance, tubes made of annealed Incoloy 800 which has been used as the reference material in the present study, has as a requirement in ASME II a value of 207 MPa for σ_{ys} and 517 MPa for σ_u at RT. Nevertheless, the actual σ_{ys} and σ_u measured in Bergant et al. (2012) were 260 and 610 MPa. Using the latter values and K_{mat} = 222 MPa m$^{1/2}$, the failure pressure ratios (now defined as the quotient of the failure pressures using minimum and actual tensile properties) are approximately 0.80 and 0.83 for plastic collapse and beginning of stable growth, respectively. Therefore, in this case the use of actual properties instead of minimum required ones can compensate the effect of degradation of the tensile properties at operating temperatures.

5. Summary of results

The main findings obtained with the FAD analyses performed in the previous sections are now summarized.

From the results presented in Figs. 2 and 4, it is clear that the effect of secondary stresses due to differential thermal expansion in typical operating conditions of PWR SGTs is reduced in terms of stability of cracks. Even when the stresses components can reach considerable values, their contribution to the total fracture driving force is, in general, small. This is in part due to the effect of mechanical stress relief effect described by the reduction of the plasticity interaction factor ϕ, Eq. (1). Therefore, acceptable integrity assessments of flawed SGTs can be obtained using solely the primary stresses.

The analyses performed in Fig. 3 show that the FAD approach can be used to predict the expected failure mode for varied configurations of cracked SGTs. Therefore, the FAD can be employed as a screening criterion enabling the selection of more adequate and precise assessment methodologies, like Elastic Plastic Fracture Mechanics for stable crack growth initiation and ductile instability or Limit Load Analysis for plastic collapse. In the case of the Fig. 3(b), it was demonstrated that a non-conservative assessment could be performed if only the traditional plastic collapse analysis is applied to relative large TWCs. This kind of mistakes can be easily avoided with a FAD methodology. Comparison with experimental information showed that the FAD is able to predict failure conditions.

Fig. 4 shows a numerical example of the evident capability of the FAD procedure to reduce the unnecessary conservatism in SGTs structural integrity assessments, even in limiting cases. The experimental results presented confirm this assumption. Actual cracks in SGTs can be located and sized more precisely nowadays, so the use of specific and more sophisticated assessments becomes more and more accessible.

Given that the previous analyses were performed with tensile and fracture properties of SGTs determined at RT, a final study of the possible effect of properties changes at higher temperature was performed. While it is well known that the tensile properties at operating temperature suffer a decrease which is easy to estimate, the behavior of the fracture toughness is still an open question. Therefore, diverse analyses were done for the most used SGT materials, Table 2, considering a reduction of tensile properties, while the fracture toughness was varied in both ways. It was observed in the comparative study that the variation of tensile properties have a higher effect on the failure condition than the variation of fracture toughness. However, it should be noted that the changes of fracture properties with temperature are not known, so this results are not conclusive.

Besides the mentioned advantages and capabilities of the FAD methodology as an assessment tool for defective SGTs, it is interesting to note their increasing and widespread use in different

industries. Hence, it is expected that the FAD will become more familiar for structural engineers facilitating their acceptance.

Perhaps the most limiting issue for accurate structural integrity assessments of cracked SGTs through the FAD approach lies in the lack of experimental results and convincing testing techniques for fracture toughness determination. Up to now, the experimental data in literature result insufficient and present some drawbacks that must be resolved (Bergant et al., 2012). The experimental research should include fracture toughness resistance curves tests for circumferential and longitudinal cracks in actual SGTs, particularly in terms of EPFM parameters as the *J*-integral or CTOD. Also high temperature tests are needed to assess flawed SGTs at operation conditions, for both tensile and fracture properties determination.

6. Conclusions

A summary of the structural integrity assessment approaches applied to flawed SGTs revealed that mainly plastic collapse analyses and, in minor extent, LEFM and EPFM methodologies were used. Hence, the FAD procedure is proposed as a comprehensive option. In order to implement the FAD analyses, tensile and fracture toughness data obtained from actual SGTs and reported in literature were employed. The evaluations were performed using a generic shape FAD curve and the API 579-1/ASME FFS-1 guide procedures.

The first FAD analyses comparing primary and secondary stresses due to typical thermal gradients in SGTs showed that the last ones have little effect on the failure condition. Then, structural integrity assessments where only primary stresses are considered seems to be enough accurate. The FAD was shown to be useful for predicting different failure modes (i.e., ductile fracture and plastic collapse) for different cracked geometries of SGTs. Also, the traditional "40% criterion" was evaluated and compared with a FAD prediction, evidencing the degree of conservatism of the former and the potentiality of the FAD methodology in order to get more accurate integrity assessments. Finally, some results about the effect of the variation of tensile and fracture properties with temperature in the FAD assessments were obtained.

The experimental data analyzed have proven that the FAD methodology is an adequate tool for assessing the structural integrity of flawed SGTs. Nevertheless, further experimental research dealing with the fracture toughness determination is needed. Testing should include specimens obtained from actual SGTs, with circumferential and longitudinal cracks at typical SG operation temperatures.

Acknowledgments

This work was supported by the Argentinean National Atomic Energy Commission (Comisión Nacional de Energía Atómica, CNEA).

Appendix A. K_I and σ_{ref} solutions for primary loads

This section presents the expressions used for calculating K_I and σ_{ref} in the previous analyses. The coefficients A_i and G_i depend on the crack geometry and were interpolated from tabular data in the API 579-1/ASME FFS-1 guide. Therefore, these values are valid only for the geometry considered in Sections 4.3–4.6.

A.1. Longitudinal TWC under internal pressure

The maximum stress intensity K_I (inside point) is

$$K_I = \frac{pR_0}{t} G_p \sqrt{\pi c}, \tag{A.1}$$

$$G_i = \frac{A_0 + A_1\lambda + A_2\lambda^2 + A_3\lambda^3}{1 + A_4\lambda + A_5\lambda^2 + A_6\lambda^3}, \tag{A.2}$$

with $A_i = (1.08;\ 0.21;\ 0.30;\ 0.00;\ 0.43;\ 0.00;\ 0.00)$.

$$\lambda = \frac{1.818c}{\sqrt{R_i t}}. \tag{A.3}$$

The reference stress σ_{ref} is:

$$\sigma_{ref} = \frac{gP_b + \left[(gP_b)^2 + 9\left(M_s P_m (1-\alpha)^2\right)^2\right]^{0.5}}{3(1-\alpha)^2}, \tag{A.4}$$

with $g = 1$, $\alpha = 0$ and $M_s = M_t$.

$$P_m = \frac{pR_i}{t}, \tag{A.5}$$

$$P_b = \frac{pR_0}{R_0^2 - R_i^2}\left[\frac{t}{R_i} - \frac{3}{2}\left(\frac{t}{R_i}\right)^2 + \frac{9}{5}\left(\frac{t}{R_i}\right)^3\right], \tag{A.6}$$

$$M_t = \left(\frac{1.02 + 0.4411\lambda^2 + 0.006124\lambda^4}{1 + 0.02642\lambda^2 + 1.533\left(10^{-6}\right)\lambda^4}\right), \tag{A.7}$$

$$\lambda = \frac{1.818c}{\sqrt{R_i a}}. \tag{A.8}$$

A.2. Longitudinal semi-elliptical PTWC under internal pressure

K_I at the deepest point of a semi-elliptical crack located in the outside surface is

$$K_I = \frac{pR_i^2}{R_0^2 - R_i^2}\left[2G_0 + 2G_1\left(\frac{a}{R_0}\right) + 3G_2\left(\frac{a}{R_0}\right)^2 + 4G_3\left(\frac{a}{R_0}\right)^3 + 5G_4\left(\frac{a}{R_0}\right)^4\right]\sqrt{\frac{\pi a}{Q}}, \tag{A.9}$$

$$G_i = \sum_{j=0}^{6} A_{j,i} \quad \text{for } i = 0 \text{ and } 1, \tag{A.10}$$

with $A_{0j} = (0.74;\ 0.04;\ 4.46;\ -8.39;\ 6.63;\ -2.07;\ -0.01)$ and $A_{1j} = (0.12;\ 0.26;\ 1.83;\ -1.59;\ 0.02;\ 0.18;\ -0.02)$ for $a/c = 0.25$ and $a/t = 0.4$. For $a/c = 0.25$ and $a/t = 0.8$, $A_{0j} = (1.29;\ -0.82;\ 10.89;\ -20.16;\ 17.61;\ -8.34;\ 1.81)$ and $A_{1j} = (0.27;\ 0.17;\ 2.51;\ -0.68;\ -4.09;\ 4.35;\ -1.44)$.

$$G_2 = \frac{\sqrt{2Q}}{\pi}\left(\frac{16}{15} + \frac{1}{3}M_1 + \frac{16}{105}M_2 + \frac{1}{12}M_3\right), \tag{A.11}$$

$$G_3 = \frac{\sqrt{2Q}}{\pi}\left(\frac{32}{35} + \frac{1}{4}M_1 + \frac{32}{315}M_2 + \frac{1}{20}M_3\right), \tag{A.12}$$

$$G_4 = \frac{\sqrt{2Q}}{\pi}\left(\frac{256}{315} + \frac{1}{5}M_1 + \frac{256}{3465}M_2 + \frac{1}{30}M_3\right), \tag{A.13}$$

$$M_1 = \frac{2\pi}{\sqrt{2Q}}(3G_1 - G_0) - \frac{24}{5}, \tag{A.14}$$

$$M_2 = 3, \tag{A.15}$$

$$M_3 = \frac{6\pi}{\sqrt{2Q}}(G_0 - 2G_1) + \frac{8}{5}, \tag{A.16}$$

$$Q = 1 + 1.464\left(\frac{a}{c}\right)^{1.65} \quad \text{for} \quad a/c < 1. \tag{A.17}$$

The reference stress σ_{ref} is calculated with Eqs. (A.4)–(A.8), where

$$\alpha = \frac{a/t}{1 + t/c}, \tag{A.18}$$

$$g = 1 - 20\left(\frac{a}{2c}\right)^{0.75}\alpha^3, \tag{A.19}$$

$$M_s = \left[1 - \frac{a}{t} + \frac{a}{t}\left(\frac{1}{M_t}\right)\right]^{-1}. \tag{A.20}$$

A.3. Circumferential TWC with net section axial force

The maximum stress intensity K_I (inside point) is

$$K_I = \frac{F}{\pi\left(R_0^2 - R_i^2\right)} G_0 \sqrt{\pi c}. \tag{A.21}$$

G_0 is calculated with Eq. (A.2) with A_i = (0.91; 0.02; 0.06; 0.00; 0.05; 0.00; 0.00).

σ_{ref} is calculated with Eq. (A.4) and $g = 1$, $P_b = 0$ and $M_s = Z$, where

$$Z = \frac{\pi\left(R_0^2 - R_i^2\right)}{(2-\tau)R_0 t\left(2\psi - \theta\right)}, \tag{A.22}$$

$$\tau = \frac{t}{R_0}, \tag{A.23}$$

$$\psi = \arccos\left(\frac{\sin\theta}{2}\right), \tag{A.24}$$

$$\theta = \frac{c}{R_m}, \tag{A.25}$$

$$\alpha = \frac{c}{\pi R_m}. \tag{A.26}$$

A.4. Circumferential semi-elliptical PTWC with net section axial force

K_I at the deepest point of a semi-elliptical crack located in the outside surface is

$$K_I = \frac{F}{\pi\left(R_0^2 - R_i^2\right)} G_0 \sqrt{\frac{\pi a}{Q}}. \tag{A.27}$$

G_0 is defined in Eq. (A.10) with A_{0j} = (0.73; 0.08; 4.03; −7.41; 5.36; −1.18; −0.25) for $a/c = 0.25$ and $a/t = 0.4$. For $a/c = 0.25$ and $a/t = 0.8$, A_{0j} = (1.05; −0.32; 7.72; −13.50; 9.00; −1.99; −0.10). Q is calculated with Eq. (A.17).

The reference stress σ_{ref} is given by Eq. (A.4) with α from Eq. (A.18), $g = 1$, $P_b = 0$ and $M_s = Z$,

$$P_m = \frac{F}{\pi\left(R_0^2 - R_i^2\right)}, \tag{A.28}$$

$$Z = \left[\frac{2\psi}{\pi} - \frac{x\theta}{\pi}\left(\frac{2 - 2\tau + x\tau}{2 - \tau}\right)\right]^{-1}, \tag{A.29}$$

$$\psi = \arccos\left(A\ \sin\theta\right), \tag{A.30}$$

$$A = x\left[\frac{(1-\tau)(2-2\tau+x\tau) + (1-\tau+x\tau)^2}{2\left\{1 + (2-\tau)(1-\tau)\right\}}\right], \tag{A.31}$$

$$\tau = \frac{t}{R_0}, \tag{A.32}$$

$$x = \frac{a}{t}, \tag{A.33}$$

$$\theta = \frac{\pi c}{4R_0}. \tag{A.34}$$

A.5. Longitudinal surface crack with infinite length under internal pressure

The stress intensity K_I for a inside crack is

$$K_I = \frac{pR_0^2}{R_0^2 - R_i^2}\left[2G_0 - 2G_1\left(\frac{a}{R_i}\right) + 3G_2\left(\frac{a}{R_i}\right)^2 - 4G_3\left(\frac{a}{R_i}\right)^3 + 5G_4\left(\frac{a}{R_i}\right)^4\right]\sqrt{\pi a}. \tag{A.35}$$

The coefficients G_i depend on the relations t/R_i (0.129 for the tube considered in 4.5) and a/t. G_i = (1.33; 0.76; 0.57; 0.47; 0.40) for $a/t = 0.2$; G_i = (1.92; 0.99; 0.69; 0.55; 0.46) for $a/t = 0.4$; G_i = (3.08; 1.41; 0.93; 0.70; 0.57) for $a/t = 0.6$ and G_i = (5.08; 2.14; 1.31; 0.95; 0.75) for $a/t = 0.8$.

The reference stress σ_{ref} is given by Eq. (A.4) with $g = 1$, P_m and P_b given by Eqs. (A.5) and (A.6) respectively, and

$$M_s = \frac{1}{1 - \alpha}, \tag{A.36}$$

$$\alpha = \frac{a}{t}. \tag{A.37}$$

Appendix B. Appendix B. K_I solutions for secondary loads

The effect of secondary stresses is introduced with the plasticity interaction factor ϕ according to Eq. (1). The relation ϕ/ϕ_0 can be obtained graphically in API 579-1/ASME FFS-1 as a function of L_r^P (load ratio based on primary stresses) and L_r^S (load ratio based on secondary stresses), and

$$\phi_0 = \left(1 + \left(\frac{1}{2\pi a}\right)\left(\frac{K_I^S}{\sigma_{ys}}\right)^2\right)^{0.5}, \tag{B.1}$$

where $a = c$ for TWCs.

Circumferential stress components (normal to longitudinal crack planes) in Fig. 1(b) were fitted with a fourth order polynomial,

$$\sigma(x) = \sigma_0 + \sigma_1\left(\frac{x}{t}\right) + \sigma_2\left(\frac{x}{t}\right)^2 + \sigma_3\left(\frac{x}{t}\right)^3 + \sigma_4\left(\frac{x}{t}\right)^4, \tag{B.2}$$

where, x is the radial component from the outside surface. The coefficients for thermal gradients $\Delta T = 50$ and 100 °C are σ_i = (−112.3; 249.6; −42.8; 8.0; −1.1) and σ_i = (−224.6; 499.1; −85.6; 15.9; −2.1), respectively.

B.1. Longitudinal TWC with fourth order polynomial stress distribution

The stress intensity factor K_I is given by

$$K_I = \left[\sigma_m G_0 + \sigma_b\left(G_0 - 2G_1\right)\right]\sqrt{\pi c}, \tag{B.3}$$

$$\sigma_m = \sigma_0 + \frac{\sigma_1}{2} + \frac{\sigma_2}{3} + \frac{\sigma_3}{4} + \frac{\sigma_4}{5}, \tag{B.4}$$

$$\sigma_b = -\frac{\sigma_1}{2} - \frac{\sigma_2}{3} - \frac{9\sigma_3}{20} - \frac{6\sigma_4}{15}. \tag{B.5}$$

G_0 and G_1 are given by Eq. (A.2) and λ from Eq. (A.3). The coefficients are A_0 = (1.00; 0.56; 0.20; 0.00; 0.21; 0.03; 0.00) and A_1 = (1.00; 1.02; 0.44; 0.03; 1.16; 0.11; 0.01).

B.2 Longitudinal semi-elliptical PTWC with fourth order polynomial stress distribution

K_I at the deepest point of a semi-elliptical crack located in the outside surface is

$$K_I = \left[G_0\sigma_0 + G_1\sigma_1\left(\frac{a}{t}\right) + G_2\sigma_2\left(\frac{a}{t}\right)^2 + G_3\sigma_3\left(\frac{a}{t}\right)^3 + G_4\sigma_4\left(\frac{a}{t}\right)^4\right]\sqrt{\frac{\pi a}{Q}}. \quad \text{(B.6)}$$

G_i and Q are calculated as in Section A.2, with the same coefficients for each crack geometry.

References

Abou-Hanna, J., McGreevy, T., Majumdar, S., 2004. Prediction of crack coalescence of steam generator tubes in nuclear power plants. Nucl. Eng. Des. 229, 175–187, ⟨http://dx.doi.org/10.1016/j.nucengdes.2003.11.011⟩.

Anderson, T., 2005. Fracture Mechanics, Fundamentals and Applications. CRC Press, Boca Raton, Florida, pp. 413.

API 579-1/ASME FFS-1, 2007. Fitness-For-Service. American Petroleum Institute and American Society of Mechanical Engineers, Washington.

ASM Handbook, 1997. Volume 19, Fatigue and Fracture. American Society for Metals International, USA, pp. 1870.

Bergant, M., Yawny, A., Perez Ipiña, J., 2012. Estimation procedure of J-resistance curves for through wall cracked steam generator tubes. Procedia Mater. Sci. 1, 273–280, ⟨http://dx.doi.org/10.1016/j.mspro.2012.06.037⟩.

Bergant, M., Yawny, A., Perez Ipiña, J., 2015. Failure assessment diagram in structural integrity analysis of steam generator tubes. Procedia Mater. Sci. 8, 128–138, ⟨http://dx.doi.org/10.1016/j.mspro.2015.04.056⟩.

Chang, Y., Kim, Y., Hwang, S., Kim, J., 2006. Burst pressure estimation of steam generator tubes based on fracture mechanics analyses. Key Eng. Mater. 321–323, 666–669, ⟨http://dx.doi.org/10.4028/www.scientific.net/KEM.321-323.666⟩.

Cizelj, L., Mavko, B., Riesch-Oppermann, H., Brucker-Froit, A., 1995. Propagation of stress corrosion cracks in steam generator tubes. Int. J. Press. Vessels Pip. 63, 35–43, ⟨http://dx.doi.org/10.1016/0308-0161(94)00046-L⟩.

EPRI TR-105505, 1997. Steam Generator Management Project, Burst Pressure Correlation for Steam Generator Tubes With Throughwall Axial Cracks. Electric Power Research Institute, Palo Alto, California (Oct).

Erhard, A., Schuler, X., Otremba, F., 2012. A new concept for steam generator tube integrity assessment. Nucl. Eng. Des. 249, 297–303, ⟨http://dx.doi.org/10.1016/j.nucengdes.2012.04.014⟩.

Flesch, B., Cochet, B., 1990. Leak-before-break in steam generator tubes. Int. J. Press. Vessels Pip. 43, 165–179, ⟨http://dx.doi.org/10.1016/0308-0161(90)90099-4⟩.

Green, S., Hetsroni, G., 1995. PWR steam generators. Int. J. Multiph. Flow 21, 1–97, ⟨http://dx.doi.org/10.1016/0301-9322(95)00016-Q⟩.

Hu, J., Liu, F., Cheng, G., Zhang, Z., 2011. Determination of the critical crack length for steam generator tubing based on fracture-mechanics-based method. Ann. Nucl. Energy 38, 1900–1905, ⟨http://dx.doi.org/10.1016/j.anucene.2011.05.009⟩.

Huh, N., Kim, J., Chang, Y., Kim, Y., Hwang, S., Kim, J., 2006. Elastic-plastic fracture mechanics assessment for steam generator tubes with through-wall cracks. Fatigue Fract. Eng. Mater. Struct. 30, 131–142, ⟨http://dx.doi.org/10.1111/j.1460-2695.2006.01094.x⟩.

IAEA-TECDOC-1577, 2007. Strategy for Assessment of WWER Steam Generator Tube Integrity. International Atomic Energy Agency, Vienna, Austria (Dec).

IAEA-TECDOC-1668, 2011. Assessment and Management of Ageing of Major Nuclear Power Plant Components Important to Safety: Steam Generators. International Atomic Energy Agency, Vienna, Austria (Update).

Kim, N., Oh, C., Kim, Y., 2010. A method to predict failure pressures of steam generator tubes with multiple through-wall cracks. Eng. Fract. Mech. 77, 842–855, ⟨http://dx.doi.org/10.1016/j.engfracmech.2009.11.007⟩.

Lee, J., Park, Y., Song, M., Kim, Y., Moon, S., 2001. Determination of equivalent single crack based on coalescence criterion of collinear axial cracks. Nucl. Eng. Des. 205, 1–11, ⟨http://dx.doi.org/10.1016/S0029-5493(00)00368-X⟩.

Majumdar, S., 1999a. Failure and leakage through circumferential cracks in steam generator tubing during accident conditions. Int. J. Press. Vessels Pip. 76, 839–847, ⟨http://dx.doi.org/10.1016/S0308-0161(99)00058-7⟩.

Majumdar, S., 1999b. Prediction of structural integrity of steam generator tubes under severe accident conditions. Nucl. Eng. Des. 194, 31–55, ⟨http://dx.doi.org/10.1016/S0029-5493(99)00168-5⟩.

Mills, W., 1987. Fracture toughness of two Ni-Fe-Cr alloys. Eng. Fract. Mech. 26, 223–238, ⟨http://dx.doi.org/10.1016/0013-7944(87)90199-8⟩.

Park, Y., Song, M., Lee, J., Moon, S., Kim, Y., 2002. Investigation on the interaction effect of two parallel axial through-wall cracks existing in steam generator tube. Nucl. Eng. Des. 214, 13–23, ⟨http://dx.doi.org/10.1016/S0029-5493(02)00010-9⟩.

Sanyal, G., Samal, M., 2013. Investigation of fracture behavior of steam generator tubes of Indian PHWR using PLT specimens. Procedia Eng. 55, 578–584, ⟨http://dx.doi.org/10.1016/j.proeng.2013.03.298⟩.

Timoshenko, S., Goodier, J., 1970. Theory of Elasticity, 3rd ed. McGraw-Hill, New York.

Tonkovic, Z., Skozrit, I., Soric, J., 2005. A contribution to assessment of steam generator tubes integrity. In: Proceedings of the 11th International Conference on Fracture, Turin, Italy.

Tonkovic, Z., Skozrit, I., Alfirevic, I., 2008. Influence of flow stress choice on the plastic collapse estimation of axially cracked steam generator tubes. Nucl. Eng. Des. 238, 1762–1770, ⟨http://dx.doi.org/10.1016/j.nucengdes.2008.01.008⟩.

Wang, X., Reinhardt, W., 2003. On the assessment of through-wall circumferential cracks in steam generator tubes with tube supports. J. Press. Vessel Technol. 125, 85–90, ⟨http://dx.doi.org/10.1115/1.1511737⟩.

Wilam, M., Cermakova, I., 1995. Integrity of VVER steam generator tubes. Theor. Appl. Fract. Mech. 23, 151–153, ⟨http://dx.doi.org/10.1016/0167-8442(95)00016-8⟩.